AGU PUBLICATIONS

Geophysical Research Letters

RESEARCH LETTER
10.1002/2017GL074133

Key Points:
- The 2016 Chiloe earthquake is a sign of the seismic reactivation of the south central Chile megathrust after the M_w 9.5 earthquake of 1960
- South central Chile has been affected by postseismic viscoelastic relaxation and superinterseismic locking after the 2010 Maule earthquake
- The Chiloe earthquake broke an ~15 km radius area at ~30 km depth, near the bottom of the seismogenic zone

Supporting Information:
- Supporting Information S1

Correspondence to:
S. Ruiz,
sruiz@dgf.uchile.cl

Citation:
Ruiz, S., M. Moreno, D. Melnick, F. del Campo, P. Poli, J. C. Baez, F. Leyton, and R. Madariaga (2017), Reawakening of large earthquakes in south central Chile: The 2016 M_w 7.6 Chiloé event, *Geophys. Res. Lett.*, *44*, 6633–6640, doi:10.1002/2017GL074133.

Received 4 FEB 2017
Accepted 14 JUN 2017
Accepted article online 19 JUN 2017
Published online 3 JUL 2017

Reawakening of large earthquakes in south central Chile: The 2016 M_w 7.6 Chiloé event

S. Ruiz[1], M. Moreno[2], D. Melnick[3], F. del Campo[4], P. Poli[5], J. C. Baez[4], F. Leyton[4], and R. Madariaga[6]

[1]Geophysics Department, Facultad de Ciencias Físicas y Matemáticas, Universidad de Chile, Santiago, Chile, [2]DeutschesGeoForschungsZentrum-GFZ, Section Lithosphere Dynamics, Potsdam, Germany, [3]Instituto de Ciencias de la Tierra, TAQUACH, Universidad Austral de Chile, Valdivia, Chile, [4]Centro Sismológico Nacional, Facultad de Ciencias Físicas y Matemáticas, Universidad de Chile, Santiago, Chile, [5]Earth and Planetary Science Department, Massachusetts Institute of Technology, Cambridge, Massachusetts, USA, [6]Laboratoire de Géologie, Ecole Normale Superieure, CNRS UMR 8538, PSL research University, Paris, France

Abstract On 25 December 2016, the M_w 7.6 Chiloé earthquake broke a plate boundary asperity in south central Chile near the center of the rupture zone of the M_w 9.5 Valdivia earthquake of 1960. To gain insight on decadal-scale deformation trends and their relation with the Chiloé earthquake, we combine geodetic, teleseismic, and regional seismological data. GPS velocities increased at continental scale after the 2010 Maule earthquake, probably due to a readjustment in the mantle flow and an apparently abrupt end of the viscoelastic mantle relaxation following the 1960 Valdivia earthquake. It also produced an increase in the degree of plate locking. The Chiloé earthquake occurred within the region of increased locking, breaking a circular patch of ~15 km radius at ~30 km depth, located near the bottom of the seismogenic zone. We propose that the Chiloé earthquake is a first sign of the seismic reawakening of the Valdivia segment, in response to the interaction between postseismic viscoelastic relaxation and changes of interseismic locking between Nazca and South America.

1. Introduction

After the occurrence of large megathrust events, it is expected that a dormant period occurs for large earthquakes in the rupture zone of megathrust faults. Such periods of quiescence have been attributed to the recovery of strength within the damaged fault zone to support stresses during the interseismic period [*Heimpel*, 1997]. For deeper events it has been suggested that the plate interface may recover its interseismic locked state rapidly, as, for example, after the Pisco 2007 M_w 8.0 and Tocopilla 2007 M_w 7.8 events [*Remy et al.*, 2016; *Weiss et al.*, 2016]. Recent observations following the Valdivia 1960 M_w 9.5 and Maule 2010 M_w 8.8 megathrust earthquakes suggest that the relocking process may be heterogeneous in space and time [*Moreno et al.*, 2011; *Métois et al.*, 2012] and accompanied by a prolonged phase of postseismic relaxation of the mantle [see, e.g., *Wang et al.*, 2012; *Ruiz et al.*, 2016, *Bedford et al.*, 2016; *Klein et al.*, 2016]. Therefore, to characterize the first indications of the seismic reawakening after the Valdivia megathrust earthquake and its associated lag time, it is essential to improve the understanding of the recurrence of earthquakes in the plate interface.

Since the 1960 Valdivia megathrust earthquake (M_w 9.5), the subduction zone in south central Chile (Figure 1) has not been affected by large earthquakes and experienced only small- to moderate-magnitude seismicity [*Lange et al.*, 2007]. The Valdivia earthquake extended for >1000 km along the plate interface [*Plafker and Savage*, 1970; *Cifuentes*, 2001; *Barrientos and Ward*, 1990; *Moreno et al.*, 2009] and produced a protracted postseismic viscoelastic relaxation observed in the regional deformation field many decades after the event [*Khazaradze et al.*, 2002; *Hu et al.*, 2004] (Figure 1). The reawakening of the south central Chile megathrust was marked by the M_w = 7.6 earthquake that occurred at 14:22:23 (UTC) on 25 December 2016 near the southwestern tip of the Chiloé Island [*Xu*, 2017]. This event was located within the southern half of the Valdivia rupture zone, close to a region that released large slip in 1960 [*Moreno et al.*, 2009].

The M_w 8.8 Maule 2010 megathrust earthquake [*Vigny et al.*, 2011; *Moreno et al.*, 2012] generated continental-scale deformation, accompanied by strain rotation and enhanced the coupling on segments adjacent to the rupture [*Klein et al.*, 2016; *Ruiz et al.*, 2016; *Melnick et al.*, 2017; *Loveless*, 2017]. This process is described as a superinterseismic phase that increases shear stress away from the rupture zone of a great earthquake,

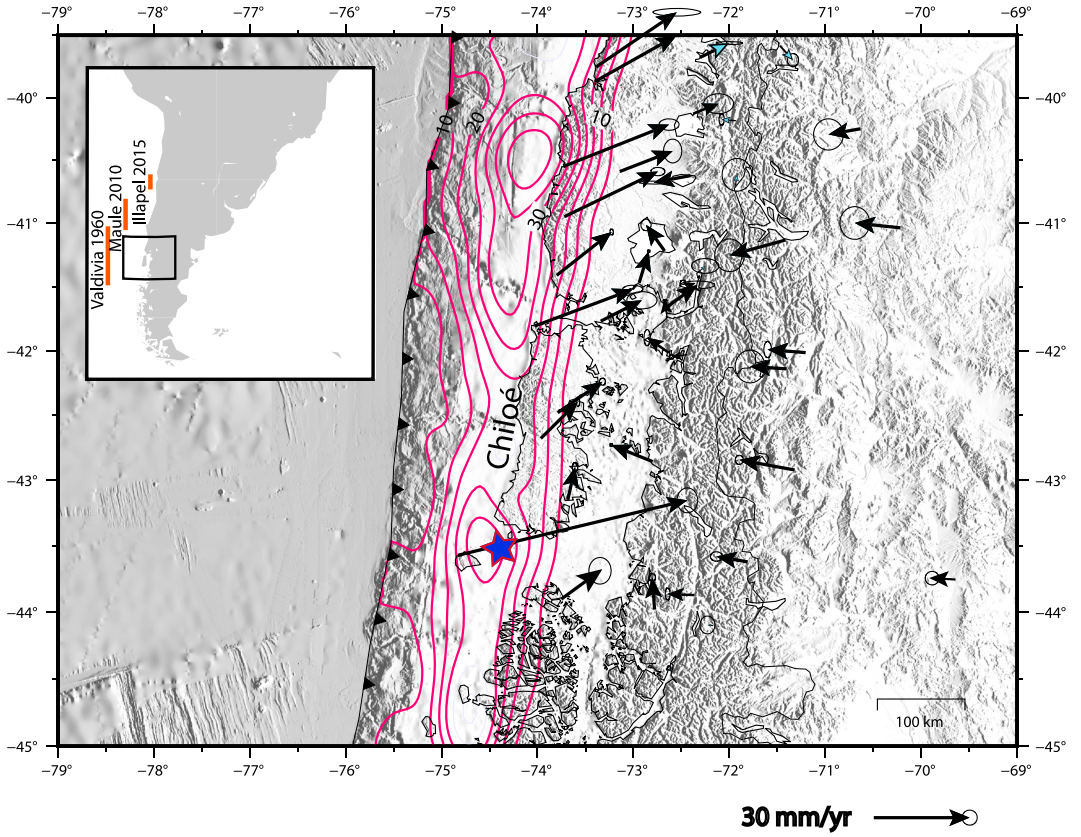

Figure 1. Regional seismotectonic setting. The purple contours show the slip distribution in meters estimated for the 1960 Valdivia earthquake [*Moreno et al.*, 2009]. Blue star is the Chilean Seismological Center (CSN) hypocenter of the 2016 Chiloé earthquake. Black vectors show GPS velocities before the 2010 Maule earthquake. Inset shows the approximate rupture length of major earthquakes discussed in the text.

bringing these areas closer to failure. It is very likely that a mechanical connection between the 2010 earthquake and the 2015 Illapel [*Ruiz et al.*, 2016; *Melnick et al.*, 2017] and 2016 Chiloé earthquakes may exist, triggering seismicity in the adjacent segments to the north and south of the 2010 rupture. In this study, we characterize the spatiotemporal evolution of surface deformation detecting velocity changes in continuous GPS time series after the 2010 Maule earthquake. Furthermore, we analyze the rupture process of the 2016 Chiloé earthquake from the inversion of regional and teleseismic data. Our goal is to characterize the reawakening of the 1960 southern segment and the possible influence of the 2010 megaearthquake on the occurrence of the 2016 Chiloé event.

2. Changes in Decadal Deformation After the 2010 Maule Earthquake in the Chiloé Region

Monitoring surface deformation using regional GPS campaigns in south central Chile started in 1993 and continued periodically during the following years together with the installation of continuously recording stations since 2005 [*Klotz et al.*, 2001; *Wang et al.*, 2007; *Moreno et al.*, 2011]. This instrumentation effort led to a detailed description of surface deformation in this region in response to different sources. The surface deformation field has been associated with the effect of postseismic mantle relaxation after the 1960 earthquake, reflected in trenchward motions observed at most inland stations [*Hu et al.*, 2004]. The coastal area, on the other hand, has experienced landward motion of variable magnitude, consistent with interseismic plate locking (Figure 1). In addition, the fore-arc region is affected by rigid block translation in response to oblique plate convergence [*Wang et al.*, 2007].

We combined all published GPS velocities [*Klotz et al.*, 2001; *Wang et al.*, 2007; *Moreno et al.*, 2011] with new estimates from cGPS to obtain a decadal deformation field. The GPS time series were computed using

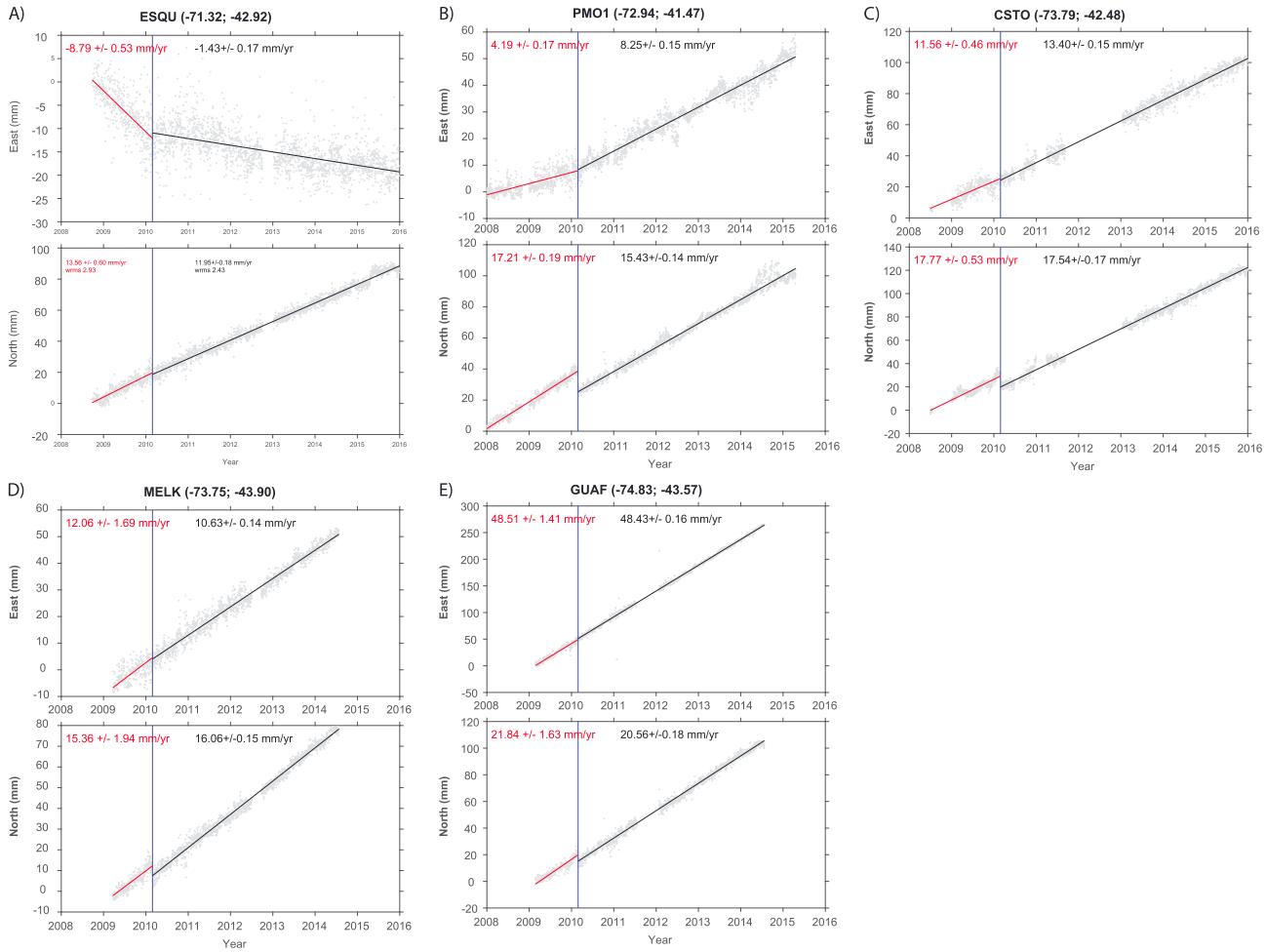

Figure 2. Daily positions and trajectory model of the GPS stations (shown in Figure 2). The labeled velocities correspond to estimates before and after the 2010 Maule earthquake within the ITRF 2008 reference frame. Red and blacks numbers are the velocities before and after the Maule earthquake of 27 February 2010, respectively. The ESQU, PM01, and CSTO sites show a significant change in the rate of eastward motion after the Maule earthquake. The MELK and GUAF sites show little velocity changes. CSTO consists of two nearby GPS sites (CSTR that recorded before 2010 and BN20 that recorded after 2010).

Bernese Global Navigation Satellite Systems (GNSS) software 5.2 [*Dach et al.*, 2015] considering International Terrestrial Reference Frame (ITRF) 2008 and South America as fixed reference frames. We followed the processing method described in *Bedford et al.* [2013] and used the Extended Linear Trajectory Model [*Bevis and Brown*, 2014] to estimate the linear trend of GPS displacements by filtering out components associated with annual and semiannual seasonal trends, Heaviside jumps caused by local earthquakes or instrumental changes, and a transient logarithmic trend resulting from viscoelastic relaxation following the 2010 Maule earthquake. GPS time series were separated in pre-2010 and post-2010 earthquake epochs in order to estimate trajectory models (Figure 2); further details of the method and trajectory models may be found in *Melnick et al.* [2017].

In order to estimate the degree of plate locking in Chiloé, we simulated the coseismic rupture of the 1960 earthquake and its postseismic viscoelastic relaxation using the methodology of *Li et al.* [2015]. The postseismic deformation model reproduces the main patterns observed in the GPS velocities before 2010. Prediction from the postseismic model was subtracted from the GPS vectors before 2010 to obtain a decadal interseismic velocity field, which was used to invert for the distribution of locking degree (Figure 3). During the last decade, locking in the Chiloé area appears to have been heterogeneously distributed, with two patches of strong locking at its southern and northern borders, separated by an area of lower locking. The 2017 Chiloé earthquake occurred in the immediate vicinity of the strongly locked southern patch (Figure 3).

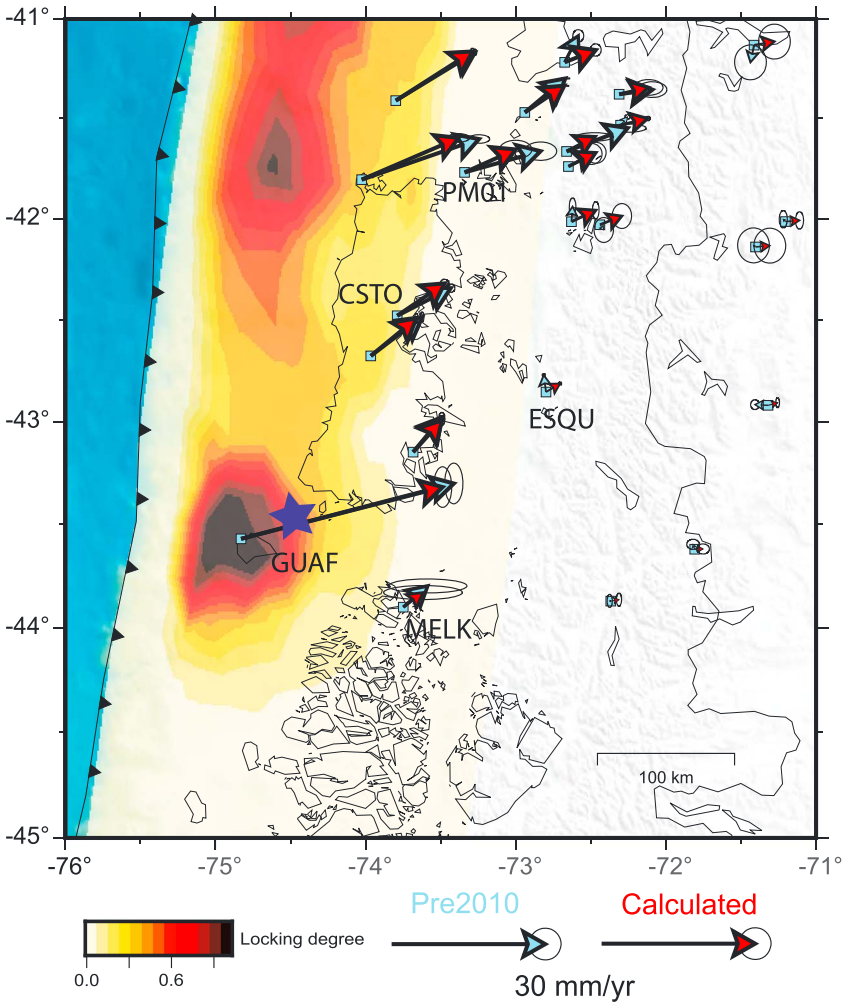

Figure 3. Degree of plate locking and velocity field before the 2010 Maule earthquake. GPS vectors have been corrected by viscoelastic relaxation following the 1960 earthquake. Blue star denotes the epicenter of Chiloé earthquake.

The overall decadal velocity field shows an increase in the velocities in the sense expected from interseismic contraction in the Chiloé region (Figure 2). Interestingly, the pattern of postseismic deformation that followed the 1960 event seems to have rapidly ended after the 2010 earthquake. This is quite clear in the time series of the cGPS station ESQU (Figure 2a). Before the 2010 Maule earthquake, ESQU was moving toward the trench at 8.97 ± 0.39 mm/yr, as a result of post-1960 mantle relaxation [*Hu et al.*, 2004]. Immediately after the 2010 earthquake, the linear velocity trend of ESQU reduced to 0.72 ± 0.12 mm/yr, probably due to a complex readjustment in mantle flow patterns, which could be interpreted as an apparent end to post-1960 mantle flow. The increase in velocities estimated at sites PM01 and CSTO (Figures 2b and 2c) located above the locked portion of the seismogenic zone suggests locally enhanced shortening rate in the upper plate, which probably reflects an increase in the degree of interseismic plate locking. On the other hand, sites MELK and GUAF (Figures 2d and 2e) show no significant variation after the 2010 earthquake, suggesting that this area has not been affected by the Maule megathrust earthquake. The large landward velocity gradient between these stations suggests a high degree of locking in the Chiloé area since at least the year 2009 (Figure 3).

3. Modeling the Rupture of the M_w 7.6, 2016 Chiloé Earthquake

3.1. Data

After the 2010 Maule megathrust earthquake in central Chile, continuously recording seismological instruments and GPS stations were deployed by the National Seismological Center of the University of Chile

(CSN). Many of these regional stations recorded the 25 December 2016 Chiloé event. We performed geodetic and kinematic source inversion, using GPS coseismic data, strong motion records, and teleseismic seismograms to model the rupture process of the M_w 7.6 Chiloé earthquake.

The regional station network that recorded the coseismic rupture is shown in Figure 4a. These are mostly multiparametric stations with collocated broadband seismometers, accelerometers, and GPS antennas, along with triggered accelerometers. Most of the broadband records were clipped, so that we used mainly the strong motion records in the modeling of the main shock. The high-rate GPS solutions were computed using the Bernese GNSS software 5.2 [*Dach et al*., 2015] in a kinematic approach using 1 Hz observations for each station. We obtain the coseismic static displacement from the kinematic solutions for stations QLLN and RMBA; for the more distant GPS stations the coseismic displacement is very close to zero. A comparison of strong motion and GPS data at collocated stations is shown in Figure 4b and shows an excellent agreement. From regional data (Figure 4), we observe an overall rupture duration of ~20 s, in agreement with the backprojection of teleseismic *P* waves recorded in North America (Figures S1 and S2 in the supporting information).

3.2. Hypocenter of the 2016 Chiloé Earthquake

The hypocenter reported by CSN is located at 43.517°S, 74.391°W, and 30 km depth (14:22:23 UTC), while that of U.S. Geological Survey (USGS) is located at 43.416°W, 73.951°W, and 35.1 km depth (14:22:26 UTC). Even if the stations used by the two agencies are the same at regional distances, the locations have an epicentral distance difference of ~50 km. We performed several tests to check which location was more plausible. We used GO07, the station closest to the epicenter, equipped with accelerometers and broadband sensors, along with the GPS antenna (QLLN) to relocate the epicenter. GO07 and QLLN are located at the same place, near the city of Quellón, at about ~50 km of the potential epicenters (Figure 4). We computed the particle motion from the GO07 strong motion records and the QLLN high-rate GPS time series to observe the direction of the first *P* arrival (Figure S3). The first *P* wave motion observed in Quellón comes from the southeast direction, the site of the hypocenter reported by CSN. We thus prefer the CSN location, obtained from the regional stations shown in Figure 4a.

3.3. Aftershocks

The large interstation distance for broadband stations prevented us from locating small-magnitude events in southern Chile (Figure 4). In general, the smallest events identified by CSN are close to local magnitude M_L 2.5 and the completeness magnitude is M_L 3.0 (Figure S4). The signal-to-noise ratio of data in the area is in general very low; this explains the large-magnitude completeness of the CSN seismological catalog. Figure 4 shows the epicenters of the events that occurred in the zone since 2010, most of the events are aftershocks of the Chiloé earthquake up to 31 January 2017. No precursory events were detected by CSN; the largest event occurred on 7 January 2016 in the northern end of the Chiloé Island at 44°S with local magnitude M_L 5.3. The aftershock seismicity is grouped in a small circular area that agrees with the slip distribution of the main shock that we propose in the next section.

3.4. Rupture Process and Slip Distribution

We use different techniques to estimate the rupture process of Chiloé earthquake. All the results show a relative simple and compact image of the rupture. The backprojection method shows a unilateral emission of radiated energy bursts extending towards the north of the epicenter for almost 30 km (Figure S2). The slip inversion using teleseismic data [*Kikuchi et al*., 1993] shows a simple rupture patch of 20 km radius and short rupture duration and a seismic moment equivalent to M_w 7.5 (Figures S5 and S6). We inverted the static displacements obtained from GPS receivers in GUAG, MELK, QLLN, and RMBA, using a uniform isotropic medium with rigidity 45 GPa and Poisson's ratio 0.25 and the slab model proposed by *Tassara and Echaurren* [2012]. This slip distribution (Figure 4) agrees well with the aftershock distribution area; the maximum slip that is larger than 4.0 m. Finally, we performed a kinematic inversion using the regional strong motion data. Given the scarcity of seismological data, we used a simplified elliptical slip distribution model to compute [*Ruiz and Madariaga*, 2013]: focal mechanism, moment magnitude, and rupture area of southern Chiloé earthquake, (Figures S7 and S8).

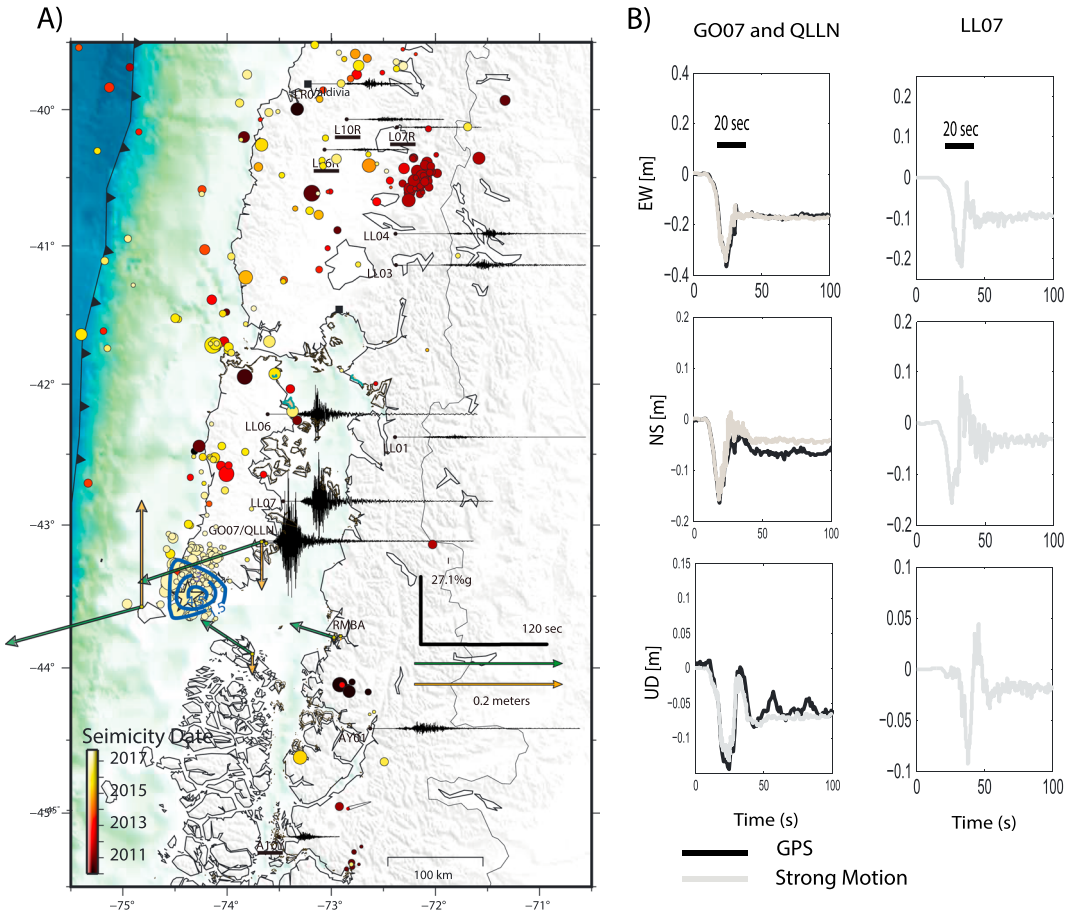

Figure 4. (a) EW components of strong motion records of the 2016 southern Chiloé main shock and coseismic static displacement of QLLN and RMBA GPS stations. Nonunderlined code names identify real-time stations that were used in the hypocenter determination by CSN and international agencies. The underlined stations code names are triggered accelerometers. Color dots correspond to the seismicity reported by CSN from 2010 to 31 January 2017; the yellow star is the main shock location. The aftershocks are grouped inside a circle of ~25 km radius in the southwestern tip of Chiloé Island. Blue isocontour lines of 1.5, 3, and 4.5 m show the result of geodetic slip inversion of Chiloé main shock. (b) GO07 and LL07 show accelerograms doubly integrated using *Boore* [2001] procedure. The displacements computed at GO07 are compared with the QLLN GPS time series. The 20 s bars highlight the duration of strong motion in these records.

4. Discussion

The observed velocity changes in the continuous GPS stations of southern Chile after the 2010 Maule earthquake show the very large scale influence of megaearthquakes on the internal deformation of tectonic plates. Here we discuss the possible link between changes of GPS velocities and viscoelastic deformation, as well as changes in interseismic locking. Before the 2010 Maule earthquake, surface deformation near the 1960 Valdivia rupture zone was dominated by viscoelastic relaxation processes following this megaearthquake [*Hu et al.*, 2004] as well as by a heterogeneous degree of plate locking throughout the rupture zone [*Moreno et al.*, 2011]. The 2010 Maule megaearthquake produced changes in the GPS velocities of sites adjacent to the rupture zone of that event at a continental scale [*Klein et al.*, 2016; *Ruiz et al.*, 2016; *Melnick et al.*, 2017] (Figure 2). *Melnick et al.* [2017] proposed that a superinterseismic phase was triggered by the Maule event in its adjacent segments, increasing the constant interseismic shear stress at the plate interface and bringing the megathrust closer to failure. These increased stresses may have contributed to triggering the M_w 8.3 Illapel earthquake (~400 km north of the 2010 rupture zone), in an area of high pre-2010 degree of interseismic locking [*Ruiz et al.*, 2016; *Klein et al.*, 2016; *Melnick et al.*, 2017]. In the southern segment, we observe a rapid change in trenchward motion of the GPS station ESQU located in the back-arc region. Interestingly, the displacement variation of this station has a similar magnitude to the predicted postseismic response after the 1960 event in this area [*Moreno et al.*, 2011]. This change in velocity cannot be attributed to

an increase in locking degree, because of the back-arc position of ESQU, well beyond the locked portion of the seismogenic zone, and because of its trenchward motion, which is opposite to motion expected from interseismic locking. We associated this sharp decrease in velocity to a complex interaction in mantle flow caused by the Valdivia 1960 and Maule 2010 megathrust earthquakes. This observation, although based on a single GPS station, may open a new approach to the understanding of mantle flow patterns and viscoelastic deformation following great earthquakes. It suggests that earthquakes in adjacent segments may change the temporal scale of postseismic deformation.

Our analysis of regional seismological and geodetic data shows that the important (~50 km) differences between the hypocenter of the USGS and the CSN agencies could be associated with different velocity models used for location, or by the fact that the CSN solution was based exclusively on the nearest stations with clear *P*, *Pn*, and *S* wave readings. The agreement between aftershocks and slip distribution models suggests that CSN proposed a more accurate rapid hypocenter location.

The hypocenter of the 2016 Chiloé earthquake is located in the deeper part of the seismogenic zone. Based on thermal modeling from a seismic refraction profile immediately north of the Chiloé rupture, *Völker et al*. [2011] proposed that the subduction slab intersects the continental Moho at 31 km depth, close to our hypocentral depth. This observation agrees with the northwest trending rupture propagation, suggesting that the earthquake nucleated at depth and subsequently propagated towards the shallower portions of the seismogenic zone. The main shock rupture was limited to a small patch of ~15 km radius, suggesting that a single connected slip patch was broken, similar to the results of *Xu* [2017] who used interferometric synthetic aperture radar data. The rupture was limited to the deeper portion of the seismogenic zone, and therefore, it only generated a small instrumental tsunami. The rupture zone occurred near the larger locked patch located in the southern part of Chiloé Island (Figure 4).

The 2016 Chiloé earthquake is the first large event that has occurred inside the rupture zone of the 1960 earthquake. The record of large earthquakes ($M_w > 7.5$) before 1960 is scarce, with very few events recorded by written historical chronicles and only large megathrust events preserved in paleoseismologic archives [*Montessus de Ballore*, 1912; *Cisternas et al*., 2005, 2017]. Historical earthquakes in the Chiloé region include the 1837 earthquake ($M \sim 8$), which in spite of its moderate magnitude generated a transpacific tsunami [*Cisternas et al*., 2017], and the 1575 earthquake that was similar to the 1960 event [*Cisternas et al*., 2005, 2017]. The 2016 Chiloé earthquake produced little structural damage in the nearest cities. We thus infer that similar seismic events lacking large tsunamis, as the 25 December event were likely ignored by the historical chronicles. The absence of such $M_w \sim 7.5$ events in the historical seismic catalogues makes it difficult to plot Gutenberg-Richter frequency magnitude curves, which are generally used to estimate the local seismic hazard. Indeed, this zone could be, by mistake, considered as an area with a low seismicity rate affected mostly by giant events separated by several centuries of quiescence.

The GPS velocity changes associated with the 2010 Maule earthquake show that distant seismogenic zones can be interconnected. Here we complement previous hypotheses based on the relation between 2010 Maule and Illapel 2015 earthquakes [*Ruiz et al*., 2016; *Klein et al*., 2016; *Melnick et al*., 2017; *Loveless*, 2017], with similar observations along the southern segment including the 2016 Chiloé event. The main difference between these two events is that Chiloé had a low seismicity rate since the 1960 Valdivia earthquake (National Earthquake Information Center) [*Lange et al*., 2007; *Poli et al*., 2017]. Here we propose that the postseismic mantle flow generated by the 1960 Valdivia event was profoundly affected by a complex interaction and possibly canceled out by opposite flow caused by the of 2010 Maule earthquake. Furthermore, we propose that the degree of plate locking in south Central Chile the Chiloé region could have increased after the 2010 earthquake during a superinterseismic phase. If this hypothesis is correct, the Chiloé earthquake can be considered as the onset of a period of higher seismic activity in south central Chile. More observations of continental-scale postseismic deformation of megaearthquakes are needed to validate our hypothesis or to propose and evaluate other more complex models.

Acknowledgments
We thank the Incorporated Research Institutions for Seismology Data Management Center and Centro Sismológico Nacional that provided the data used in this work. S.R. and R.M. thank the support of the Programa Riesgo Sísmico (AIN, Universidad of Chile) for its continuous support. S.R, J.C., and R.M. acknowledge FONDECYT 1170430. J.C. acknowledges FONDECYT 1151175. D.M acknowledges FONDECYT 1150321 and the Millennium Nucleus the Seismic Cycle Along Subduction Zones (CYCLO), ICM grant NC160025. M.M. was supported by German Science Foundation (DFG) grant MO-2310/3-1.

References

Barrientos, S., and S. Ward (1990), The 1960 Chile earthquake: Inversion for slip distribution from surface deformation, *Geophys. J. Int.*, *103*(3), 589–598, doi:10.1111/j.1365-246X.1990.tb05673.x.

Bedford, J., et al. (2013), A high-resolution, time-variable afterslip model for the 2010 Maule M_w = 8.8, Chile megathrust earthquake, *Earth Planet. Sci. Lett.*, doi:10.1016/j.epsl.2013.09.020.

Bedford, J., M. Moreno, S. Li, O. Oncken, J. C. Baez, M. Bevis, O. Heidbach, and D. Lange (2016), Separating rapid relocking, afterslip, and viscoelastic relaxation: An application of the postseismic straightening method to the Maule 2010 cGPS, *J. Geophys. Res. Solid Earth*, *121*, 7618–7638, doi:10.1002/2016JB013093.

Bevis, M., and A. Brown (2014), Trajectory models and reference frames for crustal motion geodesy, *J. Geod.*, *88*, 283–311.

Boore, D. M. (2001), Effect of baseline corrections on displacements and response spectra for several recordings of the 1999 Chi-Chi, Taiwan, earthquake, *Bull. Seismol. Soc. Am.*, *91*, 1199–1211.

Cifuentes, I. L. (1989), The 1960 Chilean earthquakes, *J. Geophys. Res.*, *94*, 665–680, doi:10.1029/JB094iB01p00665.

Cisternas, M., et al. (2005), Predecessors of the giant 1960 Chile earthquake, *Nature*, *437*(7057), 404–407, doi:10.1038/nature03943.

Cisternas, M., E. Garrett, R. Wesson, T. Dura, and L. L. Ely (2017), Unusual geologic evidence of coeval seismic shaking and tsunamis shows variability in earthquake size and recurrence in the area of the giant 1960 Chile earthquake, *Mar. Geol.*, *385*, 101–113.

Dach, R., S. Lutz, P. Walser, and P. Fridez (2015), Bernese GNSS software version 5.2, Astron. Inst., Univ. of Bern.

Heimpel, M. (1997), Critical behaviour and the evolution of fault strength during earthquake cycles, *Nature*, *388*, 856–858.

Hu, Y., K. Wang, J. He, J. Klotz, and G. Khazaradze (2004), Three-dimensional viscoelastic finite element model for postseismic deformation of the great 1960 Chile earthquake, *Geophys. Res. Lett.*, *109*, B12403, doi:10.1029/2004JB003163.

Kikuchi, M., H. Kanamori, and K. Satake (1993), Source complexity of the 1988 Armenian earthquake: Evidence for a slow after-slip event, *J. Geophys. Res.*, *98*, 15,797–15,808, doi:10.1029/93JB01568.

Khazaradze, G., K. Wang, J. Klotz, Y. Hu, and J. He (2002), Prolonged post-seismic deformation of the 1960 great Chile earthquake and implications for mantle rheology, *Geophys. Res. Lett.*, *29*(22), 2050, doi:10.1029/2002GL015986.

Klein, E., L. Fleitout, C. Vigny, and J. D. Garaud (2016), Afterslip and viscoelastic relaxation model inferred from the large-scale post-seismic deformation following the 2010 M_w 8.8 Maule earthquake (Chile), *Geophys. J. Int.*, *205*(3), 1455–1472.

Klotz, J., G. Khazaradze, D. Angermann, C. Reigber, R. Perdomo, and O. Cifuentes (2001), Earthquake cycle dominates contemporary crustal deformation in central and southern Andes, *Earth Planet. Sci. Lett.*, *193*, 437–446, doi:10.1016/S0012-821X(01)00532-5.

Lange, D., A. Rietbrock, C. Haberland, K. Bataille, T. Dahm, F. Tilmann, and E. R. Flüh (2007), Seismicity and geometry of the subduction zone of Chile between 41.5°S and 43.5°S, *Geophys. Res. Lett.*, *34*, L06311, doi:10.1029/2006GL029190.

Li, S., M. Moreno, J. Bedford, M. Rosenau, and O. Oncken (2015), Revisiting viscoelastic effects on interseismic deformation and locking degree: A case study of the Peru-North Chile subduction zone, *J. Geophys. Res. Solid Earth*, *120*, 4522–4538, doi:10.1002/2015JB011903.

Loveless, J. (2017), Super-interseismic periods: Redefining earthquake recurrence, *Geophys. Res. Lett.*, *44*, 1329–1332, doi:10.1002/2017GL072525.

Melnick, D., M. Moreno, J. Quinteros, J. C. Baez, Z. Deng, S. Li, and O. Oncken (2017), The super-interseismic phase of the megathrust earthquake cycle in Chile, *Geophys. Res. Lett.*, *44*, 784–791, doi:10.1002/2016GL071845.

Métois, M., A. Socquet, and C. Vigny (2012), Interseismic coupling, segmentation and mechanical behavior of the central chile subduction zone, *J. Geophys. Res.*, *117*, B03406, doi:10.1029/2011JB008736.

Montessus de Ballore, F. (1912), *HistoriaSísmica de los Andes Meridionales, al sur del Paralelo XVI (Cuarta Parte, Chile Central)*, pp. 1–116, Cervantes, Santiago de Chile.

Moreno, M., et al. (2011), Heterogeneous plate locking in the south-central Chile subduction zone: Building up the next great earthquake, *Earth Planet. Sci. Lett.*, *305*(3–4), 413–424, doi:10.1016/j.epsl.2011.03.025.

Moreno, M., D. Melnick, M. Rosenau, J. Baez, J. Klotz, O. Oncken, A. Tassara, J. Chen, K. Bataille, and M. Bevis (2012), Toward understanding tectonic control on the *Mw* 8.8 2010 Maule Chile earthquake, *Earth Planet. Sci. Lett.*, *321*, 152–165.

Moreno, M. S., J. Bolte, J. Klotz, and D. Melnick (2009), Impact of megathrust geometry on inversion of coseismic slip from geodetic data: Application to the 1960 Chile earthquake, *Geophys. Res. Lett.*, *36*, L16310, doi:10.1029/2009GL039276.

Plafker, G., and J. C. Savage (1970), Mechanism of the Chilean earthquake of May 21 and 22, 1960, *Geol. Soc. Am. Bull.*, *81*, 1001–1030.

Poli, P., A. Maksymowicz, and S. Ruiz (2017), The M_w 8.3 Illapel earthquake (Chile): Preseismic and postseismic activity associated with hydrated slab structures, *Geology*, doi:10.1130/G38522.1.

Remy, D., H. Perfettini, N. Cotte, J. P. Avouac, M. Chlieh, F. Bondoux, A. Sladen, H. Tavera, and A. Socquet (2016), Postseismic relocking of the subductionmegathrust following the 2007 Pisco, Peru, earthquake, *J. Geophys. Res. Solid Earth*, *121*, 3978–3995, doi:10.1002/2015JB012417.

Ruiz, S., and R. Madariaga (2013), Kinematic and dynamic inversion of the 2008 northern Iwate earthquake, *Bull. Seismol. Soc. Am.*, *103*(2A), 694–708, doi:10.1785/010120056.

Ruiz, S., et al. (2016), The seismic sequence of the 16 September 2015, Illapel M_w 8.3 earthquake, *Seismol. Res. Lett.*, doi:10.1785/0220150281.

Tassara, A., and A. Echaurren (2012), Anatomy of the Andean subduction zone: Three-dimensional density model upgraded and compared against global-scale models, *Geophys. J. Int.*, *189*(1), 161–168, doi:10.1111/j.1365-246X.2012.05397.x.

Vigny, C., et al. (2011), The 2010 M_w 8.8 Maule megathrust earthquake of central Chile, monitored by GPS, *Science*, *332*(6036), 1417–1421.

Völker, D., I. Grevemeyer, M. Stipp, K. Wang, and J. He (2011), Thermal control of the seismogenic zone of southern central Chile, *J. Geophys. Res.*, *116*, B10305, doi:10.1029/2011JB008247.

Wang, K., Y. Hu, M. Bevis, E. Kendrick, R. Smalley Jr., R. Barriga-Vargas, and E. Lauría (2007), Crustal motion in the zone of the 1960 Chile earthquake: Detangling earthquake-cycle deformation and forearc-sliver translation, *Geochem. Geophys. Geosyst.*, *8*, Q10010, doi:10.1029/2007GC001721.

Wang, K., Y. Hu, and J. He (2012), Deformation cycles of subduction earthquakes in viscoleastic Earth, *Nature*, *484*, 327–332.

Weiss, J. R., et al. (2016), Isolating active orogenic wedge deformation in the southern Subandes of Bolivia, *J. Geophys. Res. Solid Earth*, *121*, 6192–6218, doi:10.1002/2016JB013145.

Xu, W. (2017) Finite-fault slip model of the 2016 M_w 7.5 Chiloé earthquake, southern Chile, estimated from sentinel-1 data, *Geophys. Res. Lett.*, *44*, doi:10.1002/2017GL073560.